https://dx.doi.org/10.1016/j.ndteint.2021.102418

Mode Excitability and Selectivity for Enhancing Scanning Guided Wave-based Characterization of Subwavelength Defect

Kai Wang[a,b*], Ruiqi Guan[c], Yaozhong Liao[a,b], Zhongqing Su[a,b]

[a] Department of Mechanical Engineering, The Hong Kong Polytechnic University, Kowloon, Hong Kong SAR

[b] The Hong Kong Polytechnic University Shenzhen Research Institute, Shenzhen 518057, P.R. China

[c] Interdisciplinary Division of Aeronautical and Aviation Engineering, The Hong Kong Polytechnic University, Kowloon, Hong Kong SAR

Submitted to *NDT & E International*

(Initial submission on 26th June 2020; Revised and re-submitted on 10th October 2020)

* To whom correspondence should be addressed. Tel.: +852-6576-4811;
Email: kai-qf.wang@polyu.edu.hk (Kai WANG, *PhD*);

Abstract

The scanning guided ultrasonic waves (GUWs) have been exploited intensively for characterization of defects or material anomalies at their early stage. Yet, the characterization of defects in a subwavelength scale, which induces indiscernible disturbance to the linear and nonlinear features of GUWs, remains a daunting task for methods using the scanning GUWs owning to their limitation in terms of sensitivity and applicability. Based on the investigation of effect of defect on the excitability of GUW modes, we establish a framework to distinguish the optimal GUW mode with which the characterization of the small defect with subwavelength size using scanning GUWs can be enhanced. In this framework, the excitation transducer is scanned across the surface of the specimen to generate probing GUWs. The excitability of each GUW mode is analyzed, and the theoretical interpretation of effect of defect on excitation of each GUW mode is interrogated using a reciprocity theorem and Born approximation. In conjunction with the analysis of group velocity of GUW modes, the candidate GUW mode, *i.e.* mode S_1 at a frequency-thickness product of 3.58 MHz·mm, which features an excitability with optimal sensitivity to defect and high practical applicability is selected. A damage index that calibrates the extent of defect-induced variation in the waveform of the selected GUW mode is proposed, with which the subwavelength defects can be characterized accurately and reliably. Both numerical and experimental validations are performed, in which the surface and subsurface defects of subwavelength scales are identified and visualized using an imaging algorithm. The results corroborate the effectiveness of the proposed framework for enhancing the characterization of subwavelength defects using modally selective scanning GUWs.

Keywords: subwavelength defect; guided ultrasonic waves; mode excitability; nondestructive evaluation

1. Introduction

Early detection of defects (e.g. embryonic fatigue cracks, pitting corrosions, small scale voids), which is of great importance for safety-critical structures, entails high sensitivity of nondestructive evaluation approaches. This requirement is of paramount priority to warrant the integrity of components working in harsh environments and subjected to intense loading, in which defects can develop and expand rapidly. Driven by this concern, approaches that utilize transducers, in a contact [1-3] or non-contact manner [4-6], to scan inspected regions are numerous and have been widely applied. Among these approaches, conventional techniques, typified by those using the bulk wave analysis (e.g. C-scan), are confronted with multifold bottlenecks: i) limited effectiveness for structures of small thickness; ii) difficulty in resolving echoes from near-surface defects, particularly for defects of subwavelength size; and iii) challenge in resolving individual plies-induced reflections from the subwavelength defect-induced reflection in composite laminates [7, 8]. These concerns are also stressed for methods using noncontact laser-generated ultrasound, which are prevailing in specific applications requiring noncontact scanning. Therefore, the methods based on the scanning guided ultrasonic waves (GUWs), which can circumvent the above deficiencies, have been attracting intense research efforts. Via analyzing the scanning GUWs, the detection of diverse material anomalies can thereby be fulfilled with high sensitivity, owning to the rich information acquired from each wave excitation/sensing in the scanned region.

Exploiting the defect-induced disturbance in linear features and nonlinear features of probing GUWs, one can diagnose diverse material anomalies and evaluate the structural health condition qualitatively and quantitatively [9-12]. Nevertheless, the further improvement of the sensitivity of existing methods (linear or nonlinear) are limited by diverse factors related with the intrinsic features of GUWs. Using the features of defect-induced wave scattering that are of the same frequency with the incident waves, the prevailing linear GUW-based methods might overlook the defect with a scale smaller than half the wavelength of probing waves[13, 14], because the wave scattering caused by the defect is small. This deficiency can be tackled to some extent by increasing the incident frequency, but this incurs the difficulty in signal interpretation, owning to the co-existence of multimodal waves and high dispersion and attenuation of GUWs in the high frequency range. To detect small defect that does not induce great wave scattering, methods based on nonlinear features of GUWs, typified by the second harmonic generation[15-19], vibration-acoustic modulation[20, 21] and amplitude modulation phenomenon[22], have been intensively attempted. In previous investigations[15, 16, 23], we analyzed the defect-induced nonlinear features of GUWs and proposed methods to exploit them for the quantitative evaluation of small damages in two-dimensional and three dimensional scenarios and orienting the propagation direction of fatigue cracks. Despite the effectiveness of these nonlinear methods in laboratory environments, the practical measurement and calibration of the nonlinear features in probing GUWs remain a challenging task, because of their weak nature and susceptibility to interference induced by other nonlinear sources (e.g. systems and instruments) [24-27]. More importantly, material defects of certain types do not induce the material acoustic nonlinearity. For example, the pitting defects and voids in materials generated by manufacturing glitches only cause discontinuities of materials without altering material properties, inducing no nonlinear features in probing waves. Therefore, owning to the limitations in terms of sensitivity for linear methods and practical applicability for nonlinear methods, the characterization of subwavelength defects remains a daunting task.

The investigation of excitability of GUW modes can potentially offer a novel avenue for the characterization of subwavelength defects, in light of the fact that the excitability of each GUW mode can be disturbed by the defect. Investigations on the excitability of GUW modes, from theoretical and experimental perspectives, are numerous [28-34]. In some investigations, the energy enhancement when the laser pulses are in the vicinity of defects is used for the defect detection [35, 36] , and its effectiveness has been further demonstrated in FEA simulations and experiment tests [37-40]. Despite the effectiveness in detection of small scale crack [40], the detection of defects whose dimensions (i.e. length, width, depth) are all subwavelength has rarely been reported. In these investigations, the energy enhancement phenomenon is attributed to the defect-induced reflections, generation of non-propagating modes, mode conversions and wave diffraction. Nevertheless, the aspect of mode excitability has not been scrutinized, and further explicit and quantitative interpretation of defect-altered mode excitability is almost absent. Up to date, investigations dedicated to the analysis of excitability of GUW mode are only conducted in an intact waveguide, and the study and application of effect of defect on the excitation of GUW modes are rare.

In this backdrop, we develop a method based on the effect of defect on excitability of GUW modes which enhances the sensitivity and practical applicability for the characterization of defects with subwavelength sizes using scanning GUWs. The scanning GUWs are fulfilled using a scanning excitation transducer and a sensor immobilized on the specimen. This method is underpinned by the fact that for certain GUW modes, the defect-induced disturbance in excitability can be obvious at some specific frequency-thickness combinations, thereby rendering a capacity of identifying subwavelength defects. To exploit this effect to advance the evaluation of defects, an analytical interpretation of the influence of defect on the excitability of GUW modes is required, which serves as the theoretical cornerstone.

Apart from the analytical investigation on the mechanism of GUW excitability under the influence of defect, the selection of GUW mode with high applicability is also of practical significance, considering the multimodal and dispersive properties of GUWs. The selection criteria include the following two aspects. First, the selected mode-frequency combination of GUW features easy separation from other possibly excited modes. Second, the extent of defect-induced variation in the excitability shall be great, featuring an outstanding sensitivity to defects. In addition, the candidate modes in the low frequency range are preferred since they feature relatively less attenuation.

Addressing the above concerns, a framework is constructed in this investigation which is capable of selecting specific GUW modes that can significantly advance the GUW-based methods in terms of sensitivity and applicability, and thereby defects of subwavelength size can be identified. In this approach, the excitability of each GUW mode is analytically interpreted, and the defect-altered GUW excitation is investigated using the reciprocity theorem. Meanwhile, to facilitate the separation of selected GUW mode from other excited modes, the examination of group velocity is incorporated in the framework to warrant the isolation of selected GUW mode. Using this framework, the GUW mode with practical feasibility and optimal sensitivity to defects can be selected. On this basis, an index based on the proximity decorrelation is proposed to quantify the defect-induced variations in the waveforms of excited GUWs, with which the severity of the defect can be quantitatively evaluated and intuitively visualized.

2. Analytical Framework for GUW Mode Selection

2.1 Problem Description

Considering that the mechanism behind the defect-induced disturbance is essentially similar regardless of the locations of defects (e.g., surface or subsurface), the wave excitation in a plate-like waveguide bearing a surface defect is investigated without losing generality, as schematically illustrated in Fig. 1. The waves can be excited via diverse fashions, and the out-of-plane loading applied on the surface of the waveguide is considered in this study, which can be generated using piezoelectric transducers or laser pulses. In the waveguide, the incident GUWs take the modality of Lamb waves, which encompass multiple wave modes including symmetric and antisymmetric modes. A defect of subwavelength size is located on the top surface of the waveguide, representing a local thinning flaw which is a common concern for manufacturing industries. To improve the sensitivity and to enhance the reliability of the GUW-based defect detection, several key points should be addressed from both theoretical and practical perspectives. Theoretically, interpretation of the excitability of each GUW mode in the intact waveguide and the defect-induced disturbance in excitation of GUW modes provides a basis for the selection of preferred GUW mode which features high sensitivity to the defect. Practically, as multiple GUW modes co-exist in the waveguide, the precise isolation and extraction of the preferably selected GUW mode is critical for the precision and reliability of the quantitative evaluation of defect. To address a step-to-step solution to all these issues, a framework is proposed, as illustrated in the flowchart in Fig. 2. This flowchart provides an overall view of the analysis and the position of each step (Section 2.2-2.4) in the whole procedure. Via the proposed framework, the GUW modes with the capacity of identifying the subwavelength defect are selected, which feature high sensitivity to defect and appropriate group velocities. Each key step in the flowchart and each criterion are elaborated in the following sections.

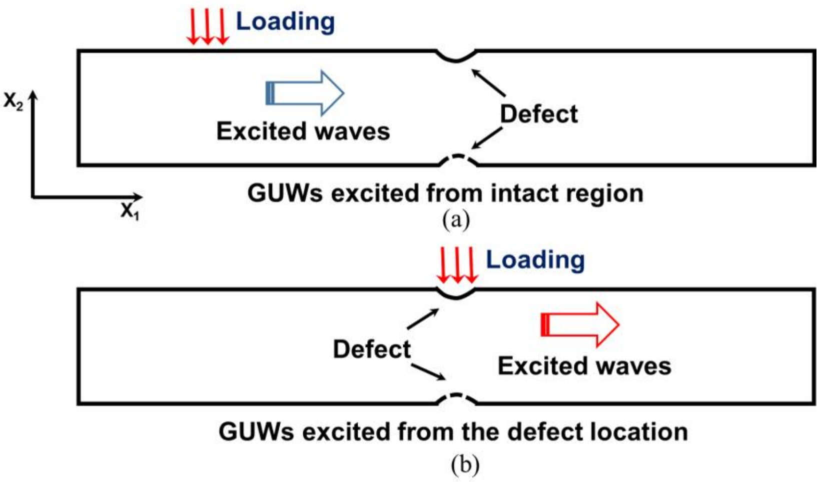

Fig. 1 Schematic illustration of excitation of GUWs (a) in the intact region and (b) at the location of surface or subsurface defect

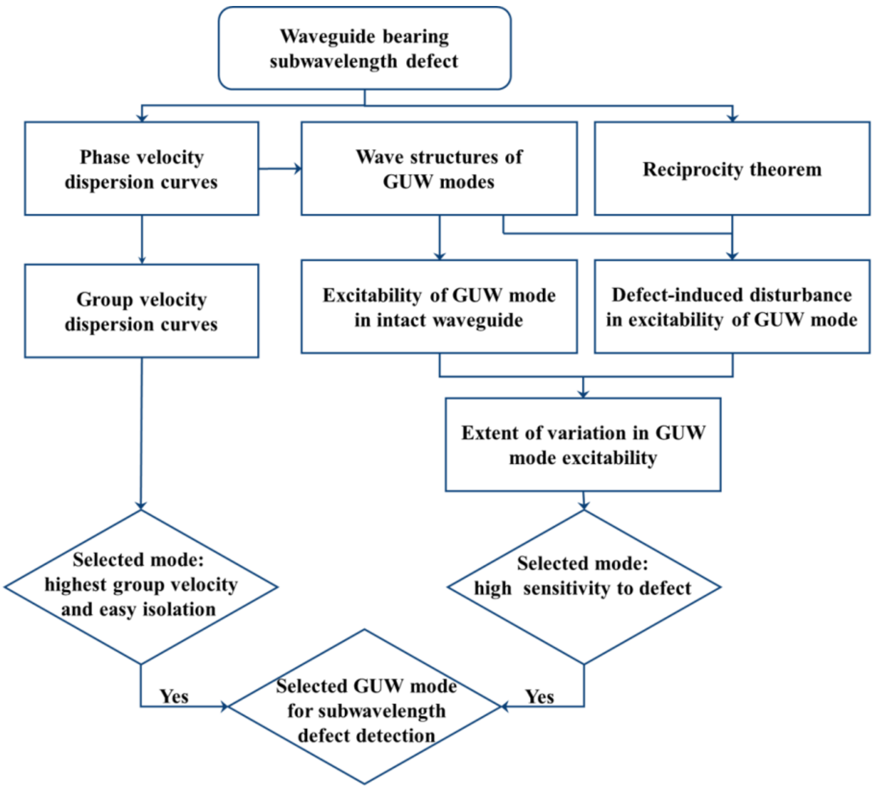

Fig. 2 Framework for the selection of GUW mode featuring high sensitivity to defect and practical feasibility

2.2 Excitability of GUW Modes in Intact Waveguide

The propagation of Lamb waves can be analytically depicted using the Rayleigh-Lamb equation, and by solving the equation via numerical methods, the phase velocity dispersion curves can be obtained. On this basis, the group velocity and the wave structure of each GUW mode can be explicitly derived. Recalling the elasto-dynamic method, a quantitative description of waves excited by the out-of-plane loading on the surface of the waveguide[30, 41], can be given as follows,

$$\mathbf{v}(x_1, x_2) = \sum_n a_n(x_1)\mathbf{v}_n(x_2) \propto \sum_n \frac{v_{2,n}(x_2)}{4P_{nn}}\mathbf{v}_n(x_2), \tag{1}$$

where $\mathbf{v}(x_1, x_2)$ is the velocity vector superposed from all the n possibly excited GUW modes, $v_{2,n}$ is the component of velocity vector in the out-of-plane loading direction for mode n. Here and hereafter, the time factor $e^{-i\omega t}$ is omitted, in which ω and t are the angular frequency and time, respectively. $a_n(x_1)$ is the amplitude. P_{nn} is the power flux of the mode n along x_1 direction, as defined in [30], and $\mathbf{v}_n(x_2)$ is the velocity vector corresponding to the P_{nn}. Provided a normalized power flux P_{nn}, the calculated value of $v_{2,n}$, a representation of mode relative excitability, at the top surface of an aluminum plate whose properties are listed in Table 1 is displayed in Fig. 3.

Table 1 Mechanical properties of the aluminum plate

Density [kg/m^3]	Elastic modulus [GPa]	Poisson's ratio	c_L [m/s]	c_T [m/s]
2660	71.8	0.33	6324	3185

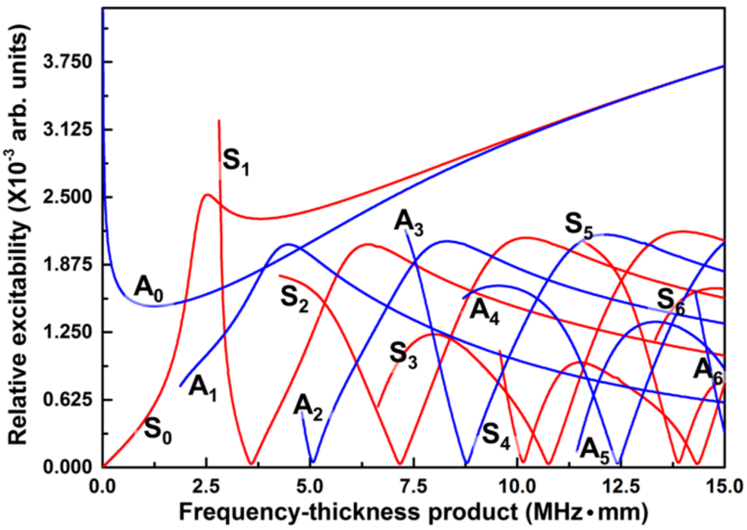

Fig. 3 Relative excitability of each Lamb mode in an intact aluminum plate

Note that, for the considered loading (out-of-plane loading on the surface), the excitability of each GUW mode varies dramatically against the incident frequency, and particularly, at some specific frequencies, the excitability of certain GUW modes is zero. This variation arises from the changes in the wave structure of each GUW mode against the incident frequency. For example, Fig. 4 representatively shows the wave structure of particulate displacement for a normalized power flux at different frequencies, from which it is clearly observed that at 4.5 MHz·mm, the out-of-plane displacement at the surface is moderately large, while at 3.58 MHz·mm, the corresponding displacement is zero. This indicates that at this specific frequency-thickness product, the out-of-plane loading exerted on the waveguide surface does not perform work on the S_1 mode. Therefore, the excitability of mode S_1 at 3.58 MHz·mm by the out-of-plane loading is minimal.

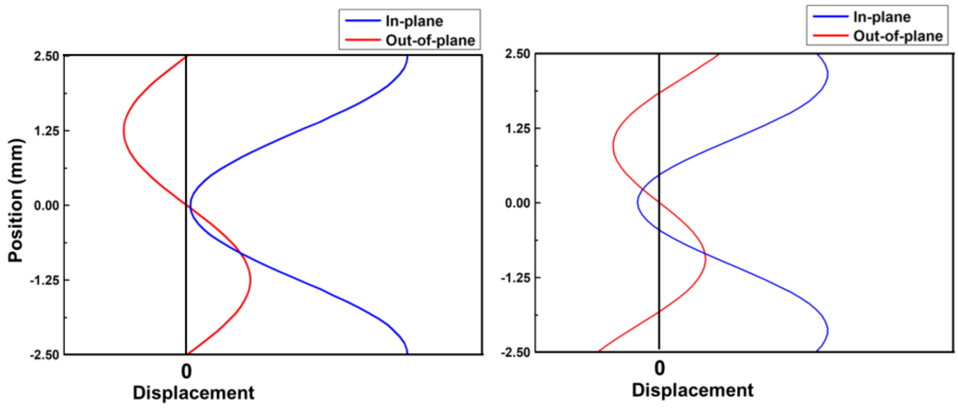

(a) (b)

Fig. 4 Wave structure of the S_1 mode at the frequency-thickness product of (a) 3.58 MHz·mm and (b) 4.5 MHz·mm in an aluminum plate

2.3 Defect-induced Disturbance in Excitability of GUW Modes

The defect-modulated excitation problem is schematically illustrated in Fig. 5. An infinite homogeneous isotropic elastic plate measuring $\boldsymbol{2h}$ in thickness bears a defect with the width $\boldsymbol{w}$ and depth $\boldsymbol{d}$ which is located on the top surface of the plate. The intact top and bottom surfaces are denoted as $\boldsymbol{S}^{+}$ and $\boldsymbol{S}^{-}$, respectively, and the surface of defect as $\boldsymbol{S}$ and the original intact surface at the defect site as $\boldsymbol{S'}$. $\boldsymbol{S}^{+}\backslash\boldsymbol{S'}$ denotes the top surface when part $\boldsymbol{S'}$ is removed. The volume of defect area bounded by $\boldsymbol{S}$ and $\boldsymbol{S'}$ is denoted as $\boldsymbol{V}$ and the region of an intact plate is denoted by $\boldsymbol{D}$. The out-of-plane loading in the intact case is a pressure of Q on the surface $\boldsymbol{S'}$, and when the loading is applied on the defect, a pressure of Q is exerted on the surface $\boldsymbol{S}$.

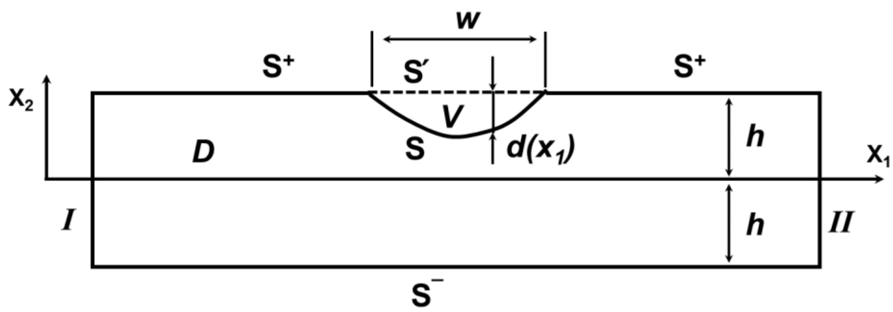

Fig. 5 Schematic illustration of waveguide bearing a surface defect

In accordance with the reciprocal theorem, two distinct elasto-dynamic states of the same body can be related via the reciprocal identity [42, 43]. For two distinct time-harmonic states, labeled by superscripts ***A*** and ***B***, the reciprocal identity for the region ***D*** bounded by the surfaces $S^{+}\backslash S'+S+S^{-}+I+II$ reads

$$\int_D \left(f_i^A u_i^B - f_i^B u_i^A \right) dv = \int_{S^{+}\backslash S'+S+S^{-}+I+II} \left(u_i^A \sigma_{ij}^B - u_i^B \sigma_{ij}^A \right) \eta_j ds. \qquad (2)$$

In the above, f_i^A and f_i^B are the body forces, u_i^A and u_i^B are the displacement fields, σ_{ij}^A and σ_{ij}^B are the stress fields, η_j are the components of the outward normal.

For the time-harmonic state denoted by ***A***, we choose a Lamb wave mode of unit power flux (denoted as $\boldsymbol{u}^{inc}=\boldsymbol{u}_n\left(x_2\right)e^{ik_n x_1}$) propagating from the left side to the right side, and after traversing the surface defect, reflected and transmitted wave modes are generated, as shown in Fig. 6. For the other state denoted by ***B***, we choose the solution when the loading is applied on the defect, generating Lamb waves of multiple modes, whose displacement field can be depicted using

$$\boldsymbol{u}^B = \sum a_m \boldsymbol{u}_m \left(x_2\right) e^{ik_m x_1}. \qquad (3)$$

For these two chosen states, the body forces are zero, and therefore the reciprocal identity reads

$$\int_{S^{+}\backslash S'+S+S^{-}+I+II} \left(u_i^A \sigma_{ij}^B - u_i^B \sigma_{ij}^A \right) \eta_j ds = 0. \qquad (4)$$

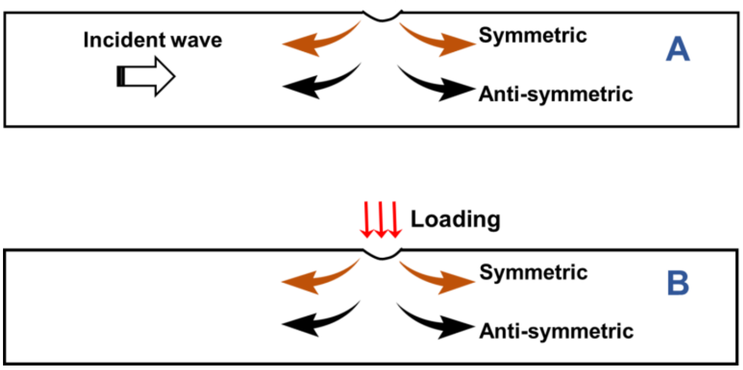

Fig. 6 Illustration of elasto-dynamic state A: a Lamb wave mode propagating from the left side to the right side; and state B: waves excited when the loading is applied at the location of defect

Considering the traction free boundary conditions for both states, the integrals over surfaces $S^+ \backslash S' + S^-$ in Eq. (4) are zero, remaining only $S + I + II$ for the Eq.(4), and thus Eq. (4) can be rewritten as

$$\int_S \left(u_i^A \sigma_{ij}^B\right) \eta_j ds + \int_{I+II} \left(u_i^A \sigma_{ij}^B - u_i^B \sigma_{ij}^A\right) \eta_j ds = 0. \tag{5}$$

Recalling the orthogonality between different Lamb modes, for the second term in Eq. (5), we have

$$\int_{I+II} \left(u_i^A \sigma_{ij}^B - u_i^B \sigma_{ij}^A\right) \eta_j ds = \int_I \left(u_i^A \sigma_{ij}^B - u_i^B \sigma_{ij}^A\right) \eta_j ds = 4 a_n P_{nn} / (-i\omega). \tag{6}$$

It is worth noting that the defect is fairly small compared with the wavelength of probing waves, leading to a negligible reflection. According to Born approximation, the wave field in state A that encompasses incident waves, reflected waves and transmitted waves, can be approximately replaced by the incident wave fields if the reflection is small enough [44]. Therefore, after some mathematical manipulations, the first term in Eq. (6) can be rewritten as

$$\begin{aligned} &\int_S \left(u_i^A \sigma_{ij}^B\right) \eta_j ds \\ &= \int_S \left[Q u_i^A \eta_i\right] ds \\ &= \int_S \left[Q u_i^{inc} \eta_i\right] ds \\ &= \int_{S+S'} \left[Q u_i^{inc} \eta_i\right] ds - \int_{S'} \left[Q u_i^{inc} \eta_i\right] ds. \end{aligned} \tag{7}$$

Substituting Eqs.(6) and (7) into Eq. (5), one can get

$$\frac{-i\omega}{4P_{nn}}\int_{S+S'}\left[Qu_i^{inc}\eta_i\right]ds = a_n - \frac{-i\omega}{4P_{nn}}\int_{S'}\left[Qu_i^{inc}\eta_i\right]ds. \tag{8}$$

Noticing that the second term on the right side of Eq. (8) is the amplitude of the wave mode excited by the loading of Q on the surface $\boldsymbol{S'}$ of the intact waveguide, and thus

$$a_n^{intact} = \frac{-i\omega}{4P_{nn}}\int_{S'}\left[Qu_i^{inc}\eta_i\right]ds. \tag{9}$$

Therefore the term on the left side of the Eq. (8) represents the deviation of the amplitude of mode n excited in the defect scenario from that in an intact scenario. In light of the Gauss's divergence theorem, the term on the left side of Eq. (8) can be further defined as

$$\frac{-i\omega}{4P_{nn}}\int_{S+S'}\left[Qu_i^{inc}\eta_i\right]ds = \frac{Q\cdot(-i\omega)}{4P_{nn}}\int_V \frac{\partial u_1^{inc}}{\partial x_1}+\frac{\partial u_2^{inc}}{\partial x_2}dv. \tag{10}$$

Recalling that the defect is fairly small compared with the wavelength of probing waves, the integrand can be approximated by the integrand at the surface of the plate, and therefore Eq.(10) can be rewritten as

$$\frac{-i\omega}{4P_{nn}}\int_{S+S'}\left[Qu^{inc}\eta_i\right]ds = \frac{Q\cdot(-i\omega)}{4P_{nn}}\left(ik\cdot u_1^{inc}+\frac{\partial u_2^{inc}}{\partial x_2}\right)\Big|_{x_2=h}\int_{-\infty}^{+\infty}h(x_1)e^{ikx_1}dx_1. \tag{11}$$

Substituting Eqs. (9) and (11) into Eq.(8) and denoting $\frac{Q\cdot(-i\omega)}{4P_{nn}}\left(ik\cdot u_1^{inc}+\frac{\partial u_2^{inc}}{\partial x_2}\right)\Big|_{x_2=h}$ as g, one has

$$a_n - a_n^{intact} = g\cdot\int_{-\infty}^{+\infty}h(x_1)e^{ikx_1}dx_1. \tag{12}$$

In the above, the term g reflects the extent of the defect-induced variation in the mode excitability, and the term $\int_{-\infty}^{+\infty}h(x_1)e^{ikx_1}dx_1$ represents the influence of the geometry of the defect on the mode excitability. With the term g in Eq.(12), the defect-induced variation in wave mode excited by the loading can be obtained, and its changes against the incident frequency is displayed in Fig. 7.

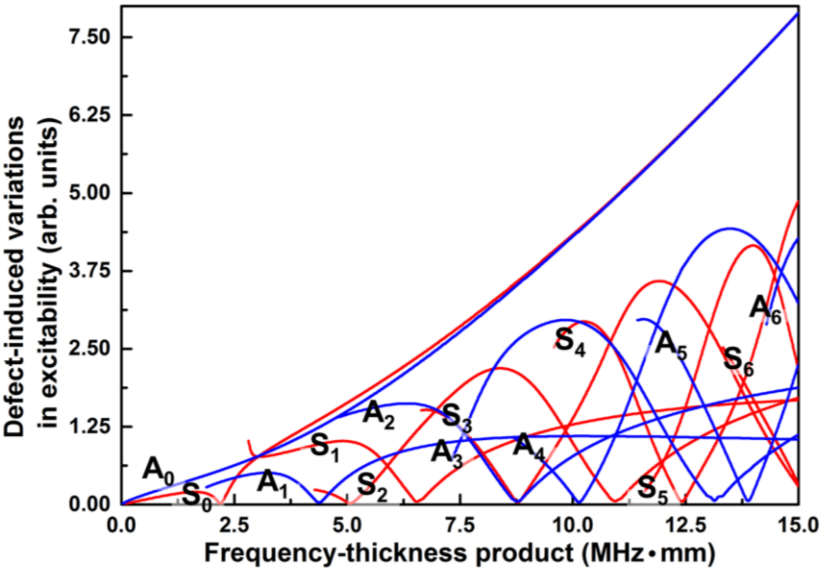

Fig. 7 Defect-induced variations in excitability of GUW modes in an aluminum plate of 5 mm thickness against the frequency

2.4 Mode Selection

To exploit the proposed GUW-based approach, it is required that the selected GUW mode features a large extent of defect-induced variation in the excitability, guaranteeing a conspicuous change in the acquired wave signals and a high sensitivity to the defect. This feature can be represented by the ratio of defect-related changes of mode excitability to the correspondent in the intact waveguide, and it can be depicted using the following

$$R = \left(a_n - a_n^{intact}\right) \Big/ a_n^{intact} \propto g \Big/ a_n^{intact} . \qquad (13)$$

With Eq.(13), the trend of the ratio against incident frequency for each GUW mode can be obtained, see Fig. 8. It is clearly observed that at several specific frequencies, the ratio is drastically larger than those for other frequencies, and thus they can serve as candidate modes with practical application potential.

Considering that multiple modes can possibly be co-excited accompanying the selected mode, group velocities of these candidate modes are to be scrutinized in the proposed framework to facilitate the practical implementation of the approach. To make the selected mode easily discernable and conveniently isolated from other modes, two requirements shall be satisfied, (1) a higher and stable group velocity in the excited frequency band and (2) the GUW with specific mode-frequency combination shall be well separated from other possibly excited GUW modes in the time domain.

Fig. 8 displays the group velocity of each GUW mode, integrated with the ratio acquired using Eq.(13). It can be clearly observed that the mode S_1 at frequency-thickness product of 3.58 MHz·mm and mode S_2 at 7.16 MHz·mm features a higher group velocity than other possibly excited modes, and the corresponding defect-related variations in excited waves are conspicuous. From the above analysis, it can be observed that these conspicuous variations arise from the wave structure features of the two modes (S_1 at 3.58 MHz·mm and S_2 at 7.16 MHz·mm) and the defect-induced variations in the in-plane load. Accommodating the requirements of sensitivity and applicability, mode S_1 at 3.58 MHz·mm and mode S_2 at 7.16 MHz·mm offer desirable selections for the GUW-based defect characterization, which enables the enhanced characterization of subwavelength defects. In addition, the mode S_1 at 3.58 MHz·mm features a lower incident frequency that is conducive to a larger inspection region. Thus it provides a preferable choice for the defect characterization and will be used in the numerical and experimental examinations. Note that the defect induces disturbance in the mode excitability in a similar mechanism regardless of the location of the defect, and thus the above analysis of mode selectivity and the preferred candidate modes also apply for the subsurface and interior defects.

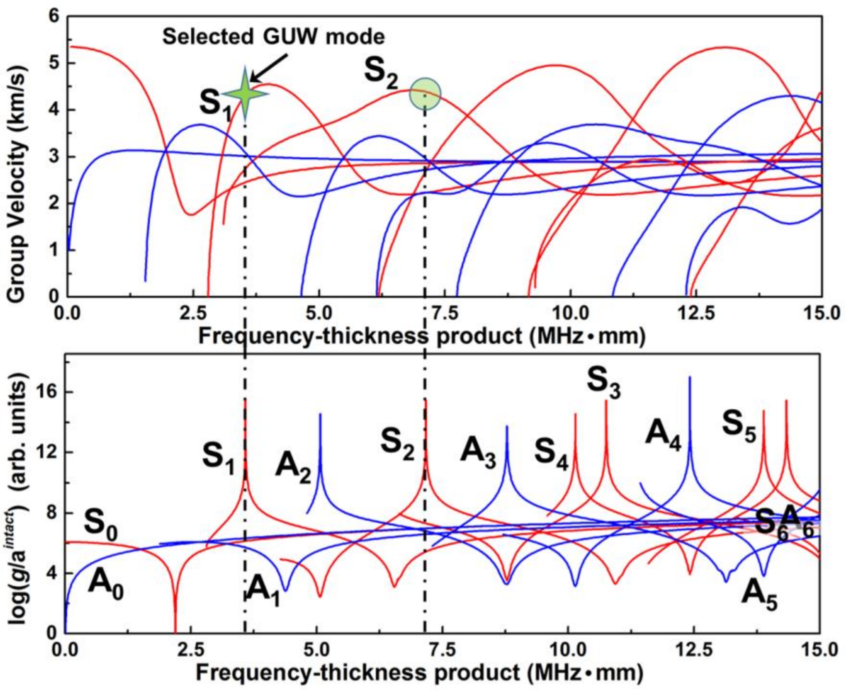

Fig. 8 Candidate GUW modes which feature easy isolation and excitability of high sensitivity to defect and: S_1 at 3.58 MHz·mm and S_2 at 7.16 MHz·mm in an aluminum plate

3. Numerical Analysis Proof-of-concept

3.1 Finite Element Model Set-up

For proof of concept, a time domain finite element analysis (FEA) is performed with ABAQUS®/Explicit. A two-dimensional plate measuring 5 mm in thickness and 1 m in length is constructed using a plane strain model, see Fig. 9, with key material properties listed in Table 1. The defect is modeled with a V-shape notch on the surface of the plate (width 2 mm, depth 0.5 mm). A global mesh of 0.1 mm size and a time step of 1×10^{-8} s are set to warrant the accuracy of the simulation results. In the FEA model, an out-of-plane loading (pressure load) is applied on the surface of the plate (within a circular area of 2 mm diameter) to excite the probing waves, which is consistent with the loading condition in the experiment. To outstand the defect-induced variation in excitability of GUW mode, the FEA analysis is performed for scenarios when the waves are excited from the intact region and locations of defects. The in-plane displacement of a sensing point on the waveguide surface with a distance of 200 mm from the loading is recorded.

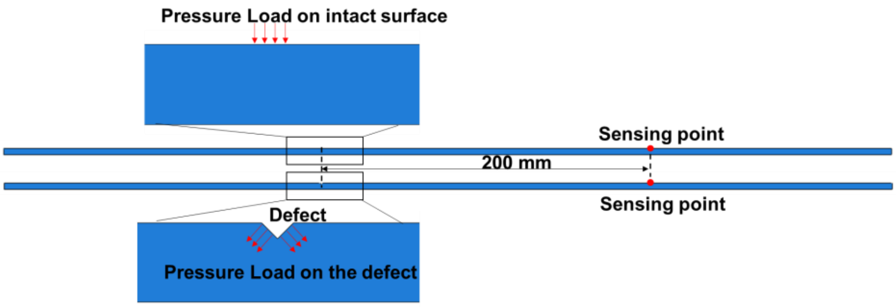

Fig. 9 FE model for validation

A one-cycle Hanning windowed toneburst with a central frequency of 0.9 MHz is first used to excite GUWs from the intact region and the defect location, respectively. This allows the examination of the excitability of the each GUW mode in both cases in a broadband low-frequency range. On this basis, the mode-frequency combinations that feature high sensitivity and high group velocity, which is predicted to be the S_1 mode at 0.716 MHz as analyzed above, can be selected for further examination of effect of defect on GUW mode excitation.

A ten-cycle Hanning windowed toneburst with the selected central frequency (predicted to be 0.716 MHz) is then applied to test the GUW mode excitation in the intact region and at the defect location, respectively. Results from both cases will be contrasted to outstand the defect-induced variations in selected GUW modes (i.e. S_1 mode).

3.2 Results: Wideband Excitation

By way of illustration, the results obtained when the excitation transducers are on the intact region and the location of a surface defect, respectively, when the one-cycle toneburst (see Fig. 10(a)) is applied, are displayed in Fig. 10(b), clearly showing the conspicuous defect-induced changes in the acquired signals. In order to evaluate the excitability of each GUW mode, the short time Fourier transform (STFT) is performed, and the spectra in the time-frequency domain is shown in Fig. 11, integrated with the dispersion curves of GUW modes. The parameters of STFT (window size 10μs and window gap 0.1μs) are prudently chosen so that sufficient details of in time and frequency domains can be retained. It is obvious that the amplitude of S_1 mode at frequency of 0.716 MHz excited in the intact case is phenomenally lower than the adjacent components, as highlighted by the circle in Fig. 11(a), arguing the above analysis that the excitability of S_1 mode at this frequency is minimal. Compared with the intact case, the S_1 mode at 0.716 MHz excited when the loading is applied on the defect is dramatically increased, as displayed in Fig. 11(b). To outstand the defect-induced changes in the excitation of each GUW mode, the spectrogram from the defect case are subtracted from that obtained from intact case, with results shown in Fig. 11(c), to observe that the defect-induced changes is drastic for S_1 mode at 0.716 MHz and mode S_2 at 1.43 MHz. A two-dimensional fast Fourier transform (2D-FFT) is performed on the signals acquired from a set of 200 points, and the difference between the spectra from the defect case and that from the intact case is shown in Fig. 11(d), further validating the above observation. This coincides well with the analytical results shown in Fig. 8, corroborating the assertion in section 2 that the extent of defect-induced variations in excitation of mode S_1 at 0.716 MHz is the greatest for the plate of 5 mm thickness, justifying its superiority for the defect evaluation in the following analysis.

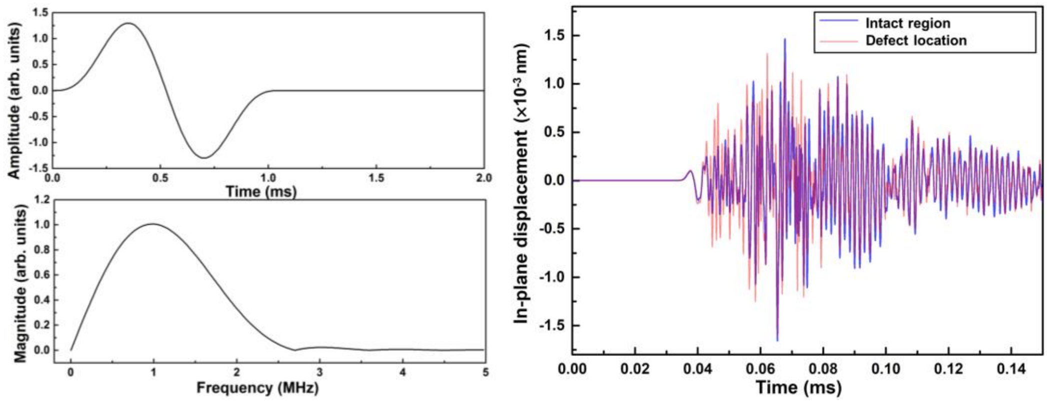

(a) (b)

Fig. 10 (a) The toneburst used for the wideband wave excitation and its spectrum and (b) the signals acquired from the sensing point

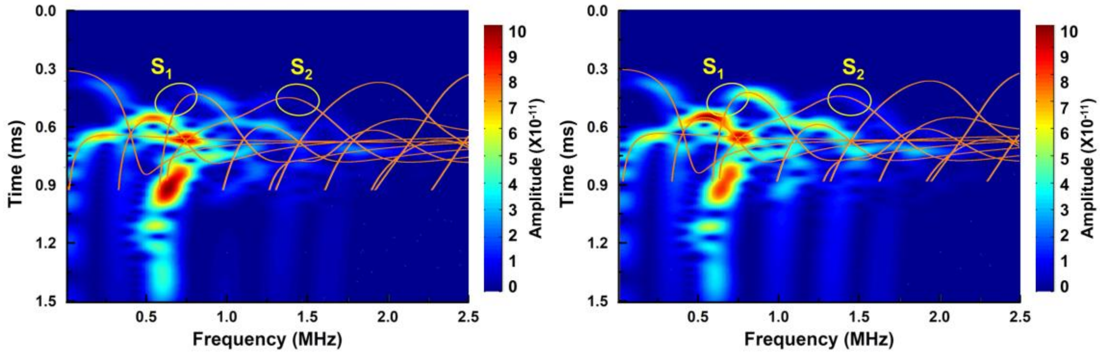

(a) (b)

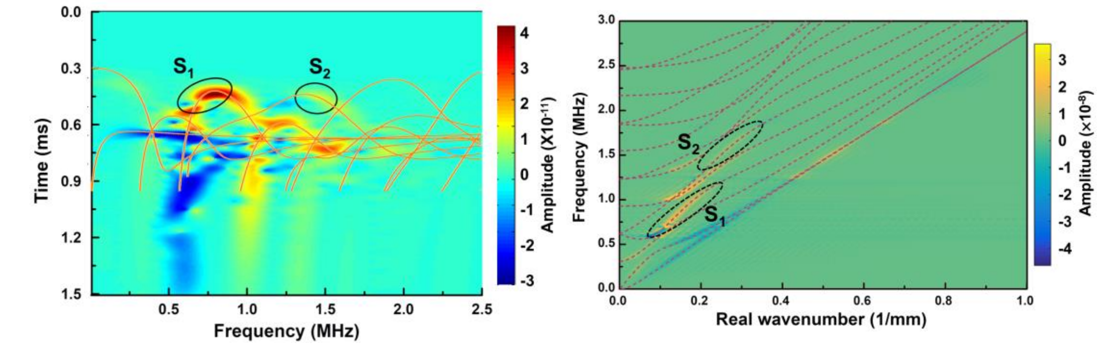

(c) (d)

Fig. 11 The STFT spectrogram of signals acquired when waves are excited from (a) intact region and (b) a defect location; (c) the result obtained by subtracting spectrogram in (b) by that in (a); (d) the result obtained by subtracting the 2D-FFT spectrogram of signals of waves excited from a defect location by that from the intact region

3.3 Results: Narrowband Harmonic Excitation

To examine the extent of the defect-induced variation in the excitation of selected mode, i.e. S_1 mode at 0.716 MHz, the ten-cycle tone burst with an identical central frequency (see Fig. 12(a)) are applied in the FEA model to excite GUWs in a narrow frequency band, as shown in Fig. 12(b). The results obtained when waves are excited from the intact region and the location of a surface defect are compared in Fig. 13(a). According to the velocity of each wave packets, it is clearly known that the first arrival wavepackets (denoted by the time window in Fig. 13(a)) are of S_1 mode, and it can be observed that in the intact case, the amplitude of S_1 mode is relatively low, while in the defect case, the corresponding amplitude is clearly increased.

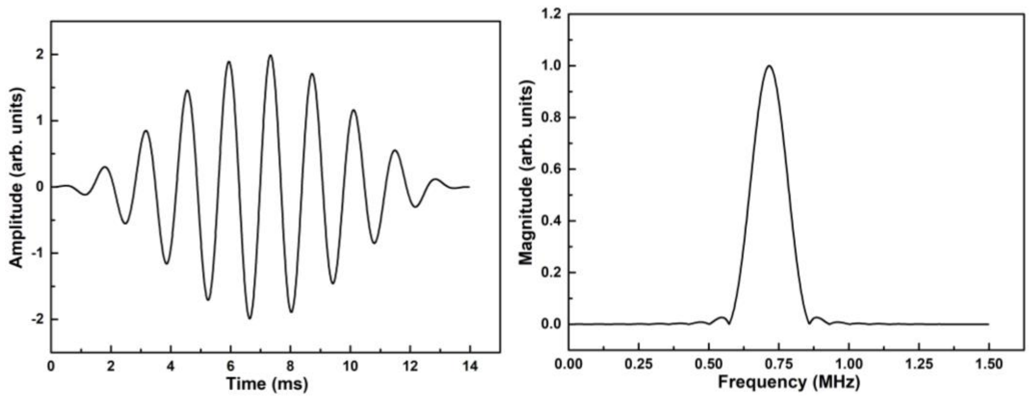

(a) (b)

Fig. 12 (a) The tone burst used for the narrowband wave excitation and (b) its spectrum

To analyze the amplitude of each GUW mode, a 2D Fourier transform is performed on the signals acquired from an array of sensing points on the surface of the waveguide, with results from the intact case and defect case shown in Fig. 13(b) and (c), respectively. The comparison clearly indicates the dramatic intensification by the defect in the excitation of S_1 mode. Subtracting the spectrogram for the intact case from that for the defect case gives the defect-induced variations in the spectral energy of each wave mode, with results shown in Fig. 13(d). The result agrees well with the theoretical analysis and the results from the wideband excitation case, validating that the excitability of selected mode features an outstanding sensitivity to the defect. The highest velocity of the S_1 mode reflects its great extractability. Note that, with the narrowband harmonic excitation, the energy of selected S_1 mode at the optimal frequency can be enhanced, thus leading to a more significant difference between the signals from cases with and without damage.

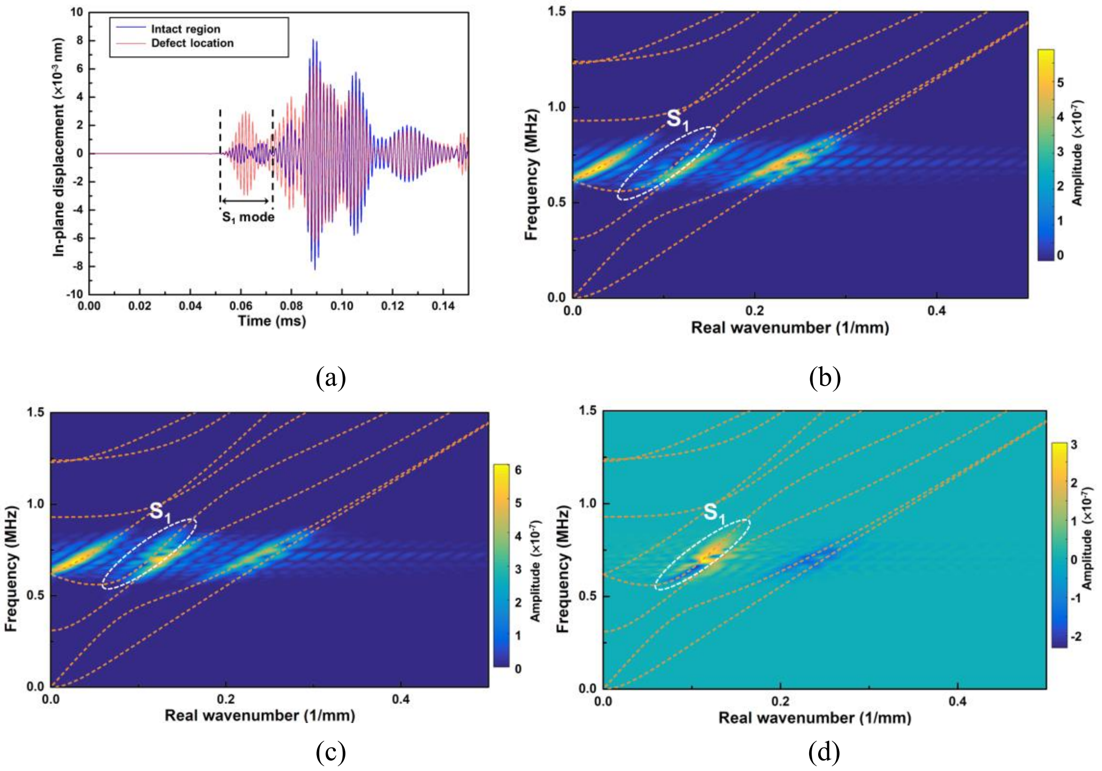

Fig. 13(a) The signals acquired when waves are excited from intact region and the location of a defect; the 2D-FFT spectrogram of signals of waves excited from (b) intact region and (c) the defect location; (d) the result obtained by subtracting spectrogram in (c) by that in (b)

Using the theoretical analysis and the FEA, the defect-induced variations in excitation of each GUW mode by the out-of-plane loading is investigated, on which basis the candidates of mode-frequency combination are selected for practical implementation. This provides the basis for the characterization of subwavelength defects with high sensitivity and practical applicability. It is noteworthy that in conventional methods, the defect is evaluated using the changes in the amplitude of GUWs, whose measurements are prone to the contaminations from diverse noises. On the contrary, the proposed method can detect the defect using the changes in the waveform of GUWs using the selected mode, as exhibited in Fig. 13(a), providing higher reliability and enhanced accuracy.

4. Experimental Validation

4.1 Experimental Set-up

An aluminum plate (Aluminum 6061-T6) measuring 5 mm in thickness whose properties are listed in Table 1 is examined experimentally. Defects with different sizes are produced on the surface of the plate using a drill. An illustration of the specimen and defects is shown in Fig. 14(a), and the diameters of the defects D1, D2, D3 and D4 are 0.5 mm, 1.5 mm, 2 mm and 0.7 mm, respectively. The depths of these defects are lower than 0.8mm.

A computer controlled system (Ritec® 5000 SNAP) is used to generate excitation signals, which are then fed into a piston piezoelectric transducer (diameter 2 mm) with central frequency of 1 MHz, as shown in Fig. 14(b), serving as an actuator to excite GUWs in the specimen. Couplant (Olympus® Glycerin) is utilized to ensure a consistent coupling between the transducer and the waveguide, via which the out-of-plane loading is transmitted onto the surface. A one-cycle Hanning-window modulated sinusoidal toneburst is used to excite waves in the plate to examine the excitability of each GUW mode in a wide frequency range. A ten-cycle Hanning-window modulated sinusoidal tone burst is then used to excite waves when the transducer scans over the inspected area covering the defects to investigate the defect-induced disturbance in the selected GUW mode, as schematically displayed in Fig. 14(b). The scanning path is denoted by the line with a distance of 2 mm between adjacent wave excitation points. A PZT wafer (2 mm x 2 mm) that measures the in-plane strain is mounted on the surface of the plate to capture the excited GUWs. To further examine the capacity of the proposed approach for the characterization of defects on the inaccessible surfaces, the ultrasonic scan with the same set-up are performed when the defects are located on the bottom surface of the plate, representing subsurface defects. Wave signals acquired from 256 measurements are averaged to suppress the measurement noises. The acquired signals are processed using the STFT to obtain the spectra.

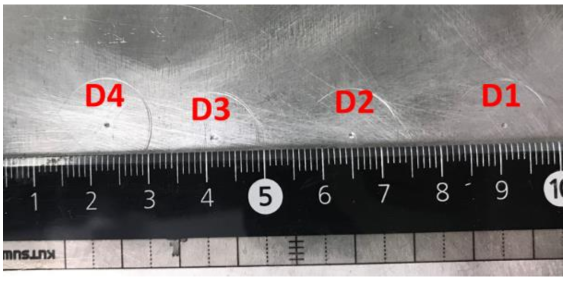

(a)

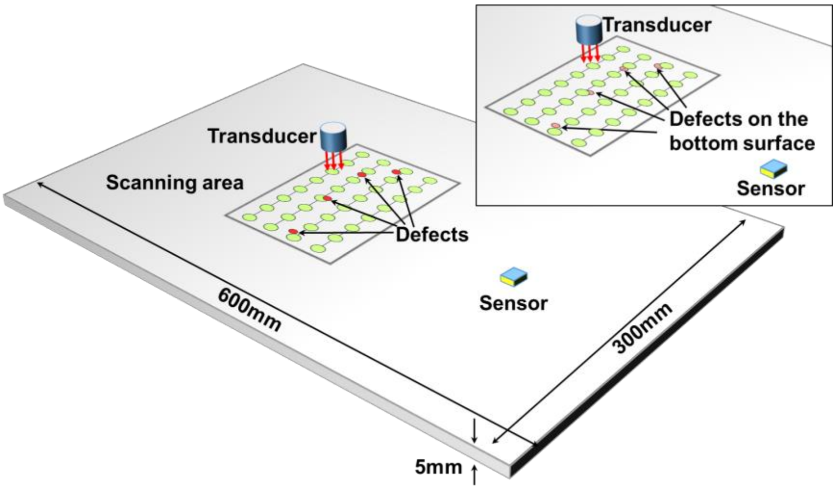

(b)

Fig. 14 Four defects of subwavelength size on the surface of an aluminum plate; (b) illustration of the set-up for the scanning test in which the defects and the transducer/sensor are on the top surface (inset: the defects are on the bottom surface)

4.2 Results and Discussions

The results when a one-cycle tone burst is used are shown in Fig. 15(a), and the corresponding spectra are displayed in Fig. 15(b) and (c). The S_1 mode at 0.716 MHz is observed to be barely excited in the intact region (see Fig. 15(b)) which agrees well with the theoretical analysis and FE analysis (see Fig. 11), and the amplitude of the excited S_1 mode at 0.716 MHz is dramatically increased when the wave excitation is altered by the defect, as shown in the Fig. 15 (c) and (d).

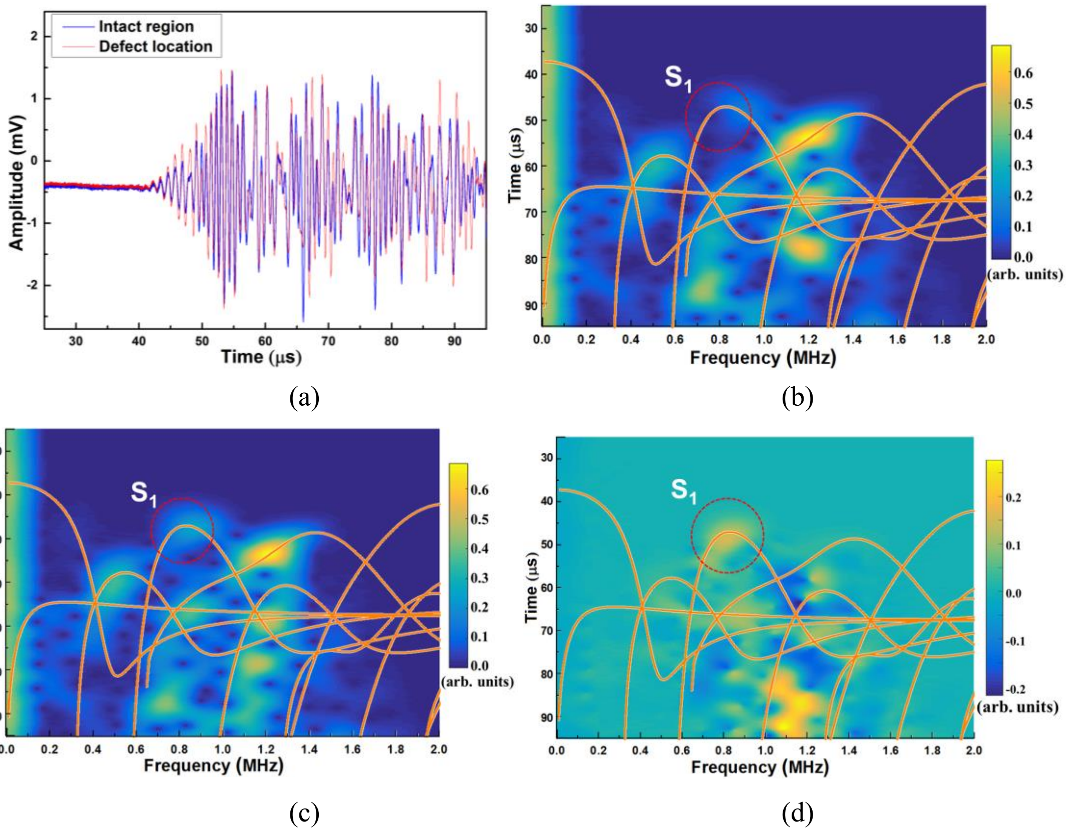

Fig. 15 (a) The signals acquired when the waves are excited from the intact region and the defect location; the STFT spectrogram of signals of waves excited from (b) intact region and (c) defect location; (d) the result obtained by subtracting spectrogram in (c) by that in (b)

As a representation, Fig. 16 shows the typical signals acquired when the ten-cycle tone burst of selected frequency (i.e. 0.716 MHz) is applied on the intact region and two of the defect locations (diameter 2 mm and 0.7 mm). It is clearly observed that the amplitude of the S_1 mode (see the signals in the denoted time window in Fig. 16) is increased by the defect, corroborating the above theoretical and FE investigations, verifying the optimal sensitivity of excitability of S_1 mode at 3.58 MHz·mm to defects.

More importantly, the waveforms of S_1 mode are dramtically changed due to the non-uniform increasing in the components at the selected frequency (i.e. 0.716 MHz in the plate of 5mm thickness) and closely adjacent frequencies. This provide the basis for the accurate and reliable imaging of the defects.

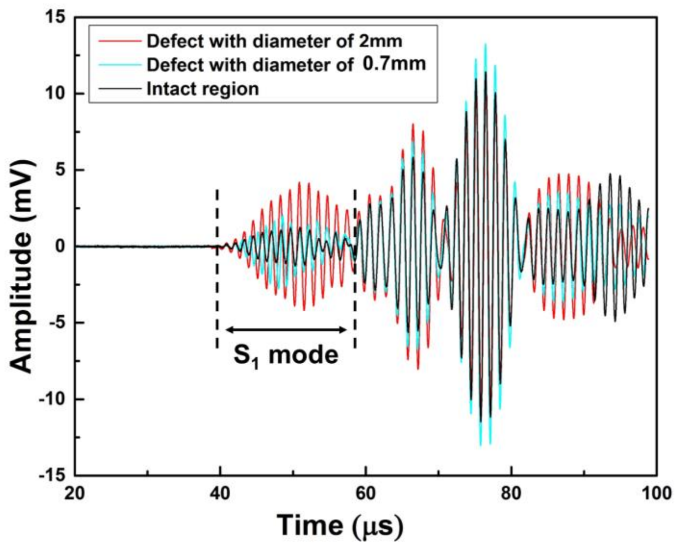

Fig. 16 The signals acquired when the waves are excited from the intact region and the defect location when the ten-cycle tone burst is applied

5. Defects Characterization and Imaging Using Damage Indices

From the above numerical and experimental investigations, it is observed that the defect induces obvious changes in the waveforms of selected wave mode, and the waves generated from spatially adjacent points in the absence of defect are highly coherent. Therefore, the defects can inversely be identified and characterized by measuring the de-coherence between signal waveforms of waves excited from adjacent points. Inspired by the stimulus to visualize and quantify the small defects, an imaging algorithm is proposed. In this algorithm, an index, based on the decorrelation between signals in specific time windows (corresponding to the S_1 mode) and generated from adjacent excitations, is developed to reflect the extent of defect-induced variations, which can be depicted as follows

$$DI_n^i = 1 - \max_{\tau} \frac{\int_{t_1}^{t_2} X_n(t) \cdot Y_i(t+\tau)\, dt}{\sqrt{\int_{t_1}^{t_2} X_n(t)^2\, dt \cdot \int_{t_1}^{t_2} Y_i(t+\tau)^2\, dt}}. \tag{14}$$

In the above, $X_n(t)$ is the signal of waves generated from the n^{th} exciting point, and $Y_i(t+\tau)$ is the signal of waves generated from the i^{th} adjacent point of the n^{th} exciting point, see Fig. 17. t_1 and t_2 denote the beginning and end of the time window for the wave packets of S_1 mode, respectively. Considering the difference in the propagation time between waves excited from the exciting point and its adjacent points, a time delay τ is applied to accommodate this difference. The indices DI_n^i represent normalized coefficients indicating the level of de-correlation in the signal waveforms of waves generated from the exciting point and the points in its proximity. Except the points at the boundary of the scanning area, a total of 8 adjacent points are used for the calculation of DI_n^i (i=1, 2, ... , 8) for each exciting point, and the mean value of these DI_n^i is defined as the damage index for the n^{th} exciting point, which can be obtained using

$$\overline{DI}_n = \frac{\sum_i DI_n^i}{8} \tag{15}$$

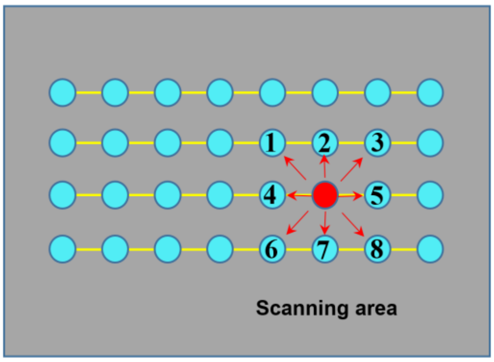

Fig. 17 Illustration of the imaging algorithm and the calculation of damage index.

In accordance with Eq.(15), the image of the entire scanned area can be constructed, and the points with outstandingly high values of $\overline{DI}$ indicate the locations of defects, which can also reflect the severity of the defect. Figure 18(a) displays the imaging results obtained using the narrowband excitation when the transducer scans over the top surface of the plate. It can be observed that the defect with a diameter not less than 0.7 mm (i.e. D2, D3 and D4) can be clearly identified, while the defect D1 with an approximated size of 0.5 mm can be barely discerned. The imaging results obtained when the defects are located on the bottom surface of the plate are shown in Fig. 18(b), to observe that the defects D2 and D3 can be detected. Nevertheless, the defects D1 and D4 cannot be discerned due to the fact that the disturbance of mode excitability induced by the defect on the bottom surface of the plate is relatively weak, making it prone to the contamination of measurement noises.

The experimental results validate the enhanced sensitivity of the proposed approach towards the characterization of subwavelength defects using scanning GUWs. Compared with conventional methods which evaluate the subtle changes in the amplitude or phase of specific modes (e.g. C-scan, energy enhancement methods) [33, 45], the proposed approach can identify the defect of a subwavelength size by evaluating the variation in the waveform of acquired signals. This endows the proposed approach a higher immunity to measurement uncertainty caused by diverse factors (e.g. couplant), thereby rendering an improved reliability. The proposed scanning GUW-based approach can also be adopted for the damage characterization in scenarios including defect in a thin plate, near-surface defects and defect in composite laminates, showing superior detectability than the conventional methods. In addition, all the signals for imaging are obtained in the current status without the need to acquire any prior knowledge, which features a baseline-free fashion, further facilitating the applicability of the proposed damage indices for characterization of defects. To further improve the sensitivity and the spatial resolution, different techniques for the wave excitation and acquisition (e.g. laser ultrasonic technique) can be exploited. For example, with the exploitation of acousto-optic modulator [35, 46], laser-generated GUWs of optimal mode can be selectively excited with a concentrated loading and thus the uncertainty related with diverse practical factors (e.g. couplant) can be eliminated. It is worth noting that the proposed method is applicable for various defects (e.g. pitting damage and shallow corrosion) regardless of their shapes and types.

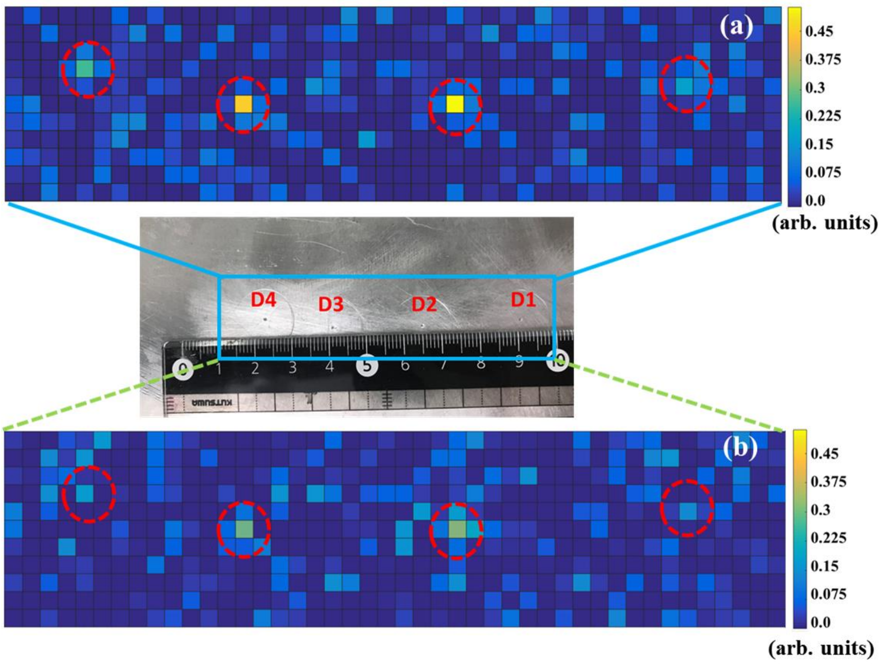

Fig. 18 The imaging results of damage index (a) when defects are located on the top surface and (b) when defects are located on the bottom surface.

6. Conclusions

Targeting enhancing the sensitivity of the scanning GUW-based method, a framework is constructed by making use of the effect of defect on the excitability of GUW modes, on which basis the GUW mode with optimal sensitivity and high applicability can be selected, enabling the characterization of subwavelength defect. In this framework, the excitability of each GUW mode is analyzed, and the effect of defect on the excitability is analytically investigated using the reciprocity theorem and the Born approximation. In conjunction with the examination of group velocity of selected candidate modes, the mode exhibiting high sensitivity and practical applicability is selected (i.e. mode S1 at 3.58 MHz·mm). Both numerical and experimental validations are performed, in which the surface and subsurface defects of subwavelength scales are identified using the modally selective scanning GUWs and visualized using an imaging algorithm. The results presented here clearly demonstrate the capability of the proposed approach to characterize the defect of subwavelength size. This approach advances the scanning GUW-based methods to a highly sensitive and practically applicable modality with the potential to provide sensitivity to previously undetectable small defects.

Acknowledgments

The work was supported by a General Project (No. 51875492) and a Key Project (No. 51635008) received from the National Natural Science Foundation of China. Z Su acknowledges the support from the Hong Kong Research Grants Council via General Research Funds (Nos. 15204419 and 15212417).

References

[1] E. Jasiūnienė, R. Raišutis, R. Šliteris, A. Voleišis, and M. Jakas, "Ultrasonic NDT of wind turbine blades using contact pulse-echo immersion testing with moving water container," *Ultragarsas" Ultrasound",* vol. 63, no. 3, pp. 28-32, 2008.

[2] W. Harizi, S. Chaki, G. Bourse, and M. Ourak, "Mechanical damage characterization of glass fiber-reinforced polymer laminates by ultrasonic maps," *Composites Part B: Engineering,* vol. 70, pp. 131-137, 2015.

[3] R. Růžek, R. Lohonka, and J. Jironč, "Ultrasonic C-Scan and shearography NDI techniques evaluation of impact defects identification," *NDT & E International,* vol. 39, no. 2, pp. 132-142, 2006.

[4] T. Hayashi, M. Murase, and M. N. Salim, "Rapid thickness measurements using guided waves from a scanning laser source," *The Journal of the Acoustical Society of America,* vol. 126, no. 3, pp. 1101-1106, 2009.

[5] S. Yashiro, J. Takatsubo, H. Miyauchi, and N. Toyama, "A novel technique for visualizing ultrasonic waves in general solid media by pulsed laser scan," *NDT & E International,* vol. 41, no. 2, pp. 137-144, 2008.

[6] L. Mallet, B. Lee, W. Staszewski, and F. Scarpa, "Structural health monitoring using scanning laser vibrometry: II. Lamb waves for damage detection," *Smart Materials and Structures,* vol. 13, no. 2, p. 261, 2004.

[7] K. S. Tan, N. Guo, B. S. Wong, and C. G. Tui, "Comparison of Lamb waves and pulse echo in detection of near-surface defects in laminate plates," *NDT & E International,* vol. 28, no. 4, pp. 215-223, 1995.

[8] J. Dong, B. Kim, A. Locquet, P. McKeon, N. Declercq, and D. Citrin, "Nondestructive evaluation of forced delamination in glass fiber-reinforced composites by terahertz and ultrasonic waves," *Composites Part B: Engineering,* vol. 79, pp. 667-675, 2015.

[9] J. Rao, A. Saini, J. Yang, M. Ratassepp, and Z. Fan, "Ultrasonic imaging of irregularly shaped notches based on elastic reverse time migration," *NDT & E International,* vol. 107, p. 102135, 2019.

[10] P. Ray, X. Yu, Z. Fan, B. Srinivasan, and P. Rajagopal, "Fiber bragg grating based detection of part-thickness cracks in bent composite laminates using feature-guided waves," *Smart Materials and Structures,* vol. 28, no. 8, p. 085026, 2019.

[11] M. Yeasin Bhuiyan, Y. Shen, and V. Giurgiutiu, "Interaction of Lamb waves with rivet hole cracks from multiple directions," *Proceedings of the Institution of Mechanical Engineers, Part C: Journal of Mechanical Engineering Science,* vol. 231, no. 16, pp. 2974-2987, 2017.

[12] C. Peng, L. Bai, J. Zhang, and B. W. Drinkwater, "The sizing of small surface-breaking fatigue cracks using ultrasonic arrays," *NDT & E International,* vol. 99, pp. 64-71, 2018.

[13] B. Masserey and P. Fromme, "In-situ monitoring of fatigue crack growth using high frequency guided waves," *NDT & E International,* vol. 71, pp. 1-7, 2015.

[14] P. Fromme, M. Lowe, P. Cawley, and P. Wilcox, "On the sensitivity of corrosion and fatigue damage detection using guided ultrasonic waves," in *IEEE Ultrasonics Symposium, 2004*, 2004, vol. 2: IEEE, pp. 1203-1206.

[15] K. Wang, M. Liu, Z. Su, S. Yuan, and Z. Fan, "Analytical insight into “breathing” crack-induced acoustic nonlinearity with an application to quantitative evaluation of contact cracks," *Ultrasonics,* vol. 88, pp. 157-167, 2018.

[16] K. Wang, Y. Li, Z. Su, R. Guan, Y. Lu, and S. Yuan, "Nonlinear aspects of “breathing” crack-disturbed plate waves: 3-D analytical modeling with experimental validation," *International Journal of Mechanical Sciences,* vol. 159, pp. 140-150, 2019.

[17] K. H. Matlack, J.-Y. Kim, L. J. Jacobs, and J. Qu, "Review of second harmonic generation measurement techniques for material state determination in metals," *Journal of Nondestructive Evaluation,* vol. 34, no. 1, p. 273, 2015.

[18] Y. Shen, J. Wang, and W. Xu, "Nonlinear features of guided wave scattering from rivet hole nucleated fatigue cracks considering the rough contact surface condition," *Smart Materials and Structures,* vol. 27, no. 10, p. 105044, 2018.

[19] Y. Shen, M. Cen, and W. Xu, "Scanning laser vibrometry imaging of fatigue cracks via

nonlinear ultrasonic guided wave scattering and mode conversion," in *Health Monitoring of Structural and Biological Systems XIII*, 2019, vol. 10972: International Society for Optics and Photonics, p. 109721I.

[20] M. Sun, Y. Xiang, M. Deng, J. Xu, and F.-Z. Xuan, "Scanning non-collinear wave mixing for nonlinear ultrasonic detection and localization of plasticity," *NDT & E International,* vol. 93, pp. 1-6, 2018.

[21] P. Liu, H. Sohn, T. Kundu, and S. Yang, "Noncontact detection of fatigue cracks by laser nonlinear wave modulation spectroscopy (LNWMS)," *NDT & E International,* vol. 66, pp. 106-116, 2014.

[22] J. Cheng, J. N. Potter, and B. W. Drinkwater, "The parallel-sequential field subtraction technique for coherent nonlinear ultrasonic imaging," *Smart Materials and Structures,* vol. 27, no. 6, p. 065002, 2018.

[23] K. Wang and Z. Su, "Analytical modeling of contact acoustic nonlinearity of guided waves and its application to evaluating severity of fatigue damage," in *Health Monitoring of Structural and Biological Systems 2016*, 2016, vol. 9805: International Society for Optics and Photonics, p. 98050L.

[24] K. Wang, W. Cao, M. Liu, Y. Li, P. Zhou, and Z. Su, "Advancing elastic wave imaging using thermal susceptibility of acoustic nonlinearity," *International Journal of Mechanical Sciences,* vol. 175, p. 105509, 2020.

[25] S. Liu, A. J. Croxford, S. A. Neild, and Z. Zhou, "Effects of experimental variables on the nonlinear harmonic generation technique," *IEEE transactions on ultrasonics, ferroelectrics, and frequency control,* vol. 58, no. 7, pp. 1442-1451, 2011.

[26] S. Roy, K. Lonkar, V. Janapati, and F.-K. Chang, "A novel physics-based temperature compensation model for structural health monitoring using ultrasonic guided waves," *Structural Health Monitoring,* vol. 13, no. 3, pp. 321-342, 2014.

[27] K.-Y. Jhang, C. J. Lissenden, I. Solodov, Y. Ohara, and V. Gusev, "Measurement of Nonlinear Ultrasonic Characteristics," ed: Springer.

[28] P. Wilcox, "Modeling the excitation of Lamb and SH waves by point and line sources," in *AIP Conference Proceedings*, 2004, vol. 700, no. 1: American Institute of Physics, pp. 206-213.

[29] Y. Shen and V. Giurgiutiu, "Excitability of guided waves in composites with PWAS transducers," in *AIP Conference Proceedings*, 2015, vol. 1650, no. 1: American Institute of Physics, pp. 658-667.

[30] J. L. Rose, *Ultrasonic guided waves in solid media*. New York: Cambridge University Press, 2014.

[31] L. Satyarnarayan, J. Chandrasekaran, B. Maxfield, and K. Balasubramaniam, "Circumferential higher order guided wave modes for the detection and sizing of cracks and pinholes in pipe support regions," *NDT & E International,* vol. 41, no. 1, pp. 32-43, 2008.

[32] D. Ratnam, K. Balasubramaniam, and B. W. Maxfield, "Generation and detection of higher-order mode clusters of guided waves (HOMC-GW) using meander-coil EMATs," *IEEE transactions on ultrasonics, ferroelectrics, and frequency control,* vol. 59, no. 4, pp. 727-737, 2012.

[33] P. Khalili and P. Cawley, "The choice of ultrasonic inspection method for the detection of corrosion at inaccessible locations," *NDT & E International,* vol. 99, pp. 80-92, 2018.

[34] P. Khalili and P. Cawley, "Excitation of single-mode Lamb waves at high-frequency-thickness

products," *IEEE transactions on ultrasonics, ferroelectrics, and frequency control,* vol. 63, no. 2, pp. 303-312, 2015.
[35] R. Pierce, C. Ume, and J. Jarzynski, "Temporal modulation of a laser source for the generation of ultrasonic waves," *Ultrasonics,* vol. 33, no. 2, pp. 133-137, 1995.
[36] Y. Sohn and S. Krishnaswamy, "A near-field scanning laser source technique and a microcantilever ultrasound receiver for detection of surface-breaking defects," *Measurement Science and Technology,* vol. 17, no. 4, p. 809, 2006.
[37] A. Clough and R. Edwards, "Characterisation of hidden defects using the near-field ultrasonic enhancement of Lamb waves," *Ultrasonics,* vol. 59, pp. 64-71, 2015.
[38] A. Clough and R. Edwards, "Scanning laser source Lamb wave enhancements for defect characterisation," *NDT & E International,* vol. 62, pp. 99-105, 2014.
[39] S. Dixon, B. Cann, D. L. Carroll, Y. Fan, and R. S. Edwards, "Non-linear enhancement of laser generated ultrasonic Rayleigh waves by cracks," *Nondestructive Testing and Evaluation,* vol. 23, no. 1, pp. 25-34, 2008.
[40] T. Hayashi and M. Fukuyama, "Vibration energy analysis of a plate for defect imaging with a scanning laser source technique," *The Journal of the Acoustical Society of America,* vol. 140, no. 4, pp. 2427-2436, 2016.
[41] B. A. Auld, *Acoustic fields and waves in solids*. Wiley, 1973.
[42] L. W. Schmerr, *Fundamentals of ultrasonic nondestructive evaluation*. Springer, 2016.
[43] J. D. Achenbach and Y. Xu, "Wave motion in an isotropic elastic layer generated by a time-harmonic point load of arbitrary direction," *The Journal of the Acoustical Society of America,* vol. 106, no. 1, pp. 83-90, 1999.
[44] Y. Da, G. Dong, B. Wang, D. Liu, and Z. Qian, "A novel approach to surface defect detection," *International Journal of Engineering Science,* vol. 133, pp. 181-195, 2018.
[45] Z. Su and L. Ye, "Lamb Wave Propagation-based Damage Identification for Quasi-isotropic CF/EP Composite Laminates Using Artificial Neural Algorithm: Part II - Implementation and Validation," *Journal of Intelligent Material Systems and Structures,* vol. 16, no. 2, pp. 113-125, 2005.
[46] S. Mezil, N. Chigarev, V. Tournat, and V. Gusev, "Two dimensional nonlinear frequency-mixing photo-acoustic imaging of a crack and observation of crack phantoms," *Journal of Applied Physics,* vol. 114, no. 17, p. 174901, 2013.